$CaCrO_3$: An Anomalous Antiferromagnetic Metallic Oxide

A. C. Komarek,[1] S. V. Streltsov,[2] M. Isobe,[3] T. Möller,[1] M. Hoelzel,[4] A. Senyshyn,[4] D. Trots,[5] M. T. Fernández-Díaz,[6] T. Hansen,[6] H. Gotou,[3] T. Yagi,[3] Y. Ueda,[3] V. I. Anisimov,[2] M. Grüninger,[1] D. I. Khomskii,[1] and M. Braden[1]

[1]*II. Physikalisches Institut, Universität zu Köln, Zülpicher Str. 77, D-50937 Köln, Germany*
[2]*Institute of Metal Physics, 620041 Ekaterinburg GSP-170, Russia*
[3]*Institute for Solid State Physics, The University of Tokyo, Chiba 277-8581, Japan*
[4]*Technische Universität Darmstadt, Material und Geowissenschaften, D-64287 Darmstadt, Germany und Technische Universität München, FRM-II, D-85747 Garching, Germany*
[5]*Hasylab/DESY, D-22607, Hamburg, Germany*
[6]*Institut Laue-Langevin, 38042 Grenoble, France*

(Received 16 March 2008; revised manuscript received 7 May 2008; published 16 October 2008)

Combining infrared reflectivity, transport, susceptibility, and several diffraction techniques, we find compelling evidence that $CaCrO_3$ is a rare case of a metallic and antiferromagnetic transition-metal oxide with a three-dimensional electronic structure. Local spin density approximation calculations correctly describe the metallic behavior as well as the anisotropic magnetic ordering pattern of *C* type: The high Cr valence state induces via sizable *pd* hybridization remarkably strong next-nearest-neighbor interactions stabilizing this ordering. The subtle balance of magnetic interactions gives rise to magnetoelastic coupling, explaining pronounced structural anomalies observed at the magnetic ordering transition.

DOI: 10.1103/PhysRevLett.101.167204 PACS numbers: 75.10.−b, 71.15.−m, 75.25.+z, 78.20.−e

Strongly correlated electron systems including the wide class of transition-metal oxides (TMOs) exhibit a quite general relation between magnetic order and electrical conductivity [1]: ferromagnetism typically coexists with metallic conductivity, whereas insulators usually exhibit antiferromagnetism. It is always a challenge to understand exceptions from this rule. The rare observations of ferromagnetism in insulating TMOs most often are due to a particular type of orbital ordering [2]. The few examples of antiferromagnetic (AFM) metals, e.g., $(La/Sr)_3Mn_2O_7$ [3] or $Ca_3Ru_2O_7$ [4], are characterized by reduced electronic and structural dimensionality, and the AFM order corresponds to a stacking of ferromagnetic (FM) layers. Here we report the discovery of a three-dimensional transition-metal oxide with metallic conductivity, AFM exchange interactions, and *C*-type AFM order: the perovskite $CaCrO_3$.

Perovskites containing Cr^{4+} ($CaCrO_3$, $SrCrO_3$, and $PbCrO_3$) were already studied previously [5–10], but neither the details of the crystal structure nor the nature of the magnetic ordering are known. Only very recently evidence for *C*-type AFM order was reported in multiphase samples of $SrCrO_3$ [10]. Regarding the conductivity, the existing data are controversial. In Refs. [7,9] $CaCrO_3$ was claimed to be metallic, but more recently insulating behavior has been reported [5]. A similar controversy persists for $SrCrO_3$, which should definitely be more metallic than $CaCrO_3$ due to the less distorted crystal structure, but metallic behavior was observed in Ref. [5] only under pressure.

$CaCrO_3$ exhibits an orthorhombic $GdFeO_3$-type perovskite structure. Early magnetization measurements indicate a magnetic transition at 90 K [8], which is confirmed in our samples. Two electrons occupy the Cr $3d$ shell ($S = 1$), rendering the material electronically similar to insulating RVO_3 [11] (also $3d^2$) and to metallic $(Ca/Sr)RuO_3$ [12]. In $CaCrO_3$, the valence of Cr^{4+} is unusually high, which may lead to a small or even negative charge-transfer gap Δ [13,14], i.e., holes in the O band. In CrO_2 the negative Δ leads to self-doping [15] and to a ferromagnetic metallic state. In contrast, layered Sr_2CrO_4 with $\sim$180° Cr-O-Cr bonds is an AFM insulator with a gap of $\sim$0.2 eV [16].

Combining diffraction, macroscopic and infrared reflectivity measurements with local spin density approximation (LSDA) and LSDA + U calculations we have studied the properties of $CaCrO_3$. We find that $CaCrO_3$ is an antiferromagnetic metallic transition-metal oxide with a *C*-type magnetic structure. According to LSDA calculations, the magnetic order arises from competing nearest-neighbor (NN) and next-nearest-neighbor (NNN, ''diagonal'') exchange interactions, which result from a sizable *pd* hybridization. Remarkably, the magnetic transition at $T = 90$ K causes pronounced anomalies in structural and transport properties.

Polycrystalline $CaCrO_3$ was prepared by a solid state reaction of CaO and CrO_2 under 4 GPa at 1000 °C for 30 min. The obtained samples of stoichiometric reactions always include a varying amount of the impurities of Cr_2O_3 and $CaCr_2O_4$ (see also [8]). A small excess of CaO (5–10%), however, almost completely eliminated these impurities, and the excess CaO could be washed out with distilled water. Close inspection showed that single-crystalline grains of up to 0.1 mm diameter were obtained by this procedure as well. Powder neutron measurements were performed on the SPODI diffractometer at the FRM-II ($\lambda = 1.548$ Å) as well as on D20 at the ILL

($\lambda = 2.4233$ Å). Lattice parameters have been studied with synchrotron radiation at the beam line B2 at Hasylab/DESY ($\lambda = 0.75$ Å) for temperatures between 15 and 1063 K. A sample decomposition, however, allowed us to obtain reliable data only up to ~800 K. X-ray single-crystal structure analysis was performed on a Bruker X8-Apex diffractometer using Mo $- K_\alpha$ radiation between 90 and 300 K. In spite of twining a satisfactory intensity integration was achieved due to the small splitting of the pseudocubic parameters. Final intensity R-values were 2%–4%. These data confirm the close to perfect stoichiometry of our samples. The electrical resistivity $\rho(T)$ was measured by an AC four-point method on a pellet which was cold-pressed at 12.5 kbar. The infrared reflectivity $R(\omega)$ of a cold-pressed pellet was determined from 7 to 900 meV using a Fourier spectrometer. As reference we used *in situ* Au evaporation.

The lattice parameters determined by synchrotron-radiation powder diffraction are shown in Fig. 1. All three orthorhombic parameters exhibit a steplike anomaly at the magnetic ordering temperature determined by SQUID susceptibility and neutron diffraction measurements, $T_N =$ 90 K. Although the sudden changes in the lattice constants are rather strong, up to 0.5% for c, there is no visible effect in the lattice volume. Whereas c shrinks, a and b elongate upon cooling, yielding a flattening of the *Pbnm* structure. There is no evidence for phase mixture. Close inspection of the temperature dependence suggests that this flattening already starts at much higher temperatures.

The neutron powder and the x-ray single-crystal experiments give the full structural information including the positional and the displacement parameters, from which all bond angles and distances can be calculated (see Fig. 2). The $GdFeO_3$-type structure (space group *Pbnm*) develops out of the ideal perovskite structure by rotating, angle Φ, and tilting, angle Θ, the CrO_6 octahedra [17]. Between 3.5 and 300 K, $\Theta = 10.5°$ and $\Phi = 8.2°$ are nearly constant, reflecting a sizable structural distortion. The combination of tilt and rotation yields two distinct O positions: apical O1 out-of-plane and O2 in the *ab* plane. Regarding a distortion of the basal plane of the octahedron, we do not find a splitting in the Cr-O2 distances but a weak temperature independent elongation of the octahedron parallel to a; i.e., the O2-O2 edges are different (see Fig. 2). In addition, we find an overall flattening of the octahedron following the flattening of the lattice at T_N: The Cr-O1 (Cr-O2) distance shrinks (elongates) upon cooling. The compression of the octahedron points to a temperature-driven redistribution amongst the t_{2g} orbitals increasing the d_{xy} occupation upon cooling into the magnetically ordered state. In electronically similar Ca_2RuO_4, a similar (but

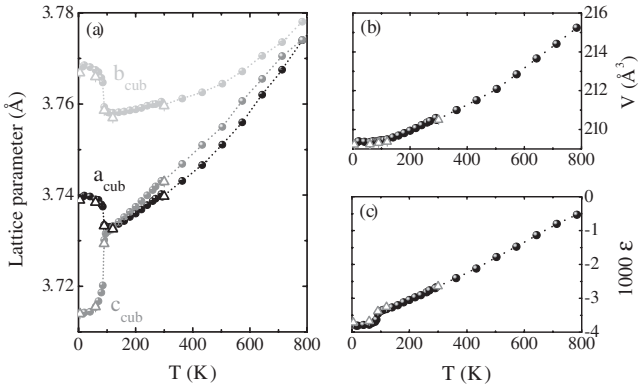

FIG. 1. (a) Orthorhombic lattice parameters a, b, and c, scaled to the parameter of a cubic perovskite: $a_{cub} = a/\sqrt{2}$, $b_{cub} = b/\sqrt{2}$ and $c_{cub} = c/2$. (b) and (c) show the orthorhombic splitting ε and the lattice volume V. Circles refer to synchrotron and triangles to neutron diffraction results.

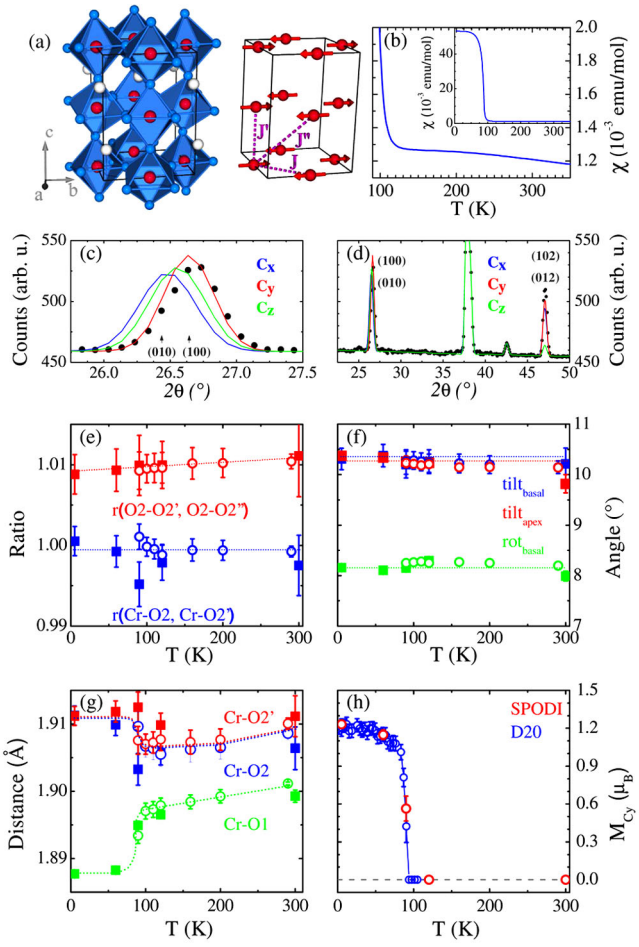

FIG. 2 (color online). (a) Crystal structure of $CaCrO_3$ in space group *Pbnm* and the *C*-type magnetic structure of Cr moments (*red*) indicating the main magnetic interaction paths. (b) Magnetic susceptibility. (c)–(h) Results of powder neutron (*squares*) and single-crystal x-ray (*circles*) measurements. (c) Magnetic (010)/(100) reflection at 3.5 K and calculated profiles for C_x, C_y and C_z type magnetic order. (d) Part of the neutron diffraction pattern at 3.5 K and calculated profiles. (e) Ratio of O2-O2 and Cr-O2 bond lengths; (f) Octahedral tilt Θ and rotation Φ angles. (g) Cr-O1 and Cr-O2 bond lengths. (h) C_y-type ordered magnetic moment in μ_B.

larger) flattening of the octahedron has been attributed to a pronounced orbital rearrangement [18,19].

Below $T_N = 90$ K two strong magnetic peaks emerge at (100) and (102)/(012) which can unambiguously be attributed to C_y-type AFM order; see Fig. 2. Other schemes fail to yield the correct peak positions or intensity ratio. In space group $Pbnm$ the C_y-type order may couple with F_x and G_z components according to the irreducible representation Γ_{2g} [20]. The F_x component perfectly agrees with the observation of weak ferromagnetism in the susceptibility; see Fig. 2(b). We find a sizable ordered moment of $1.2\mu_B$ at low temperature.

The resistivity $\rho(T)$ exhibits $\partial\rho/\partial T < 0$ but a rather small value at 300 K, 0.1 Ω m (see inset of Fig. 3). Furthermore, $\rho(T)$ does not diverge towards low T but tends to a finite value. Upon a first cooling cycle we find a clear jump at T_N most likely due to cracks caused by the pronounced structural anomalies. A similar jump was observed close to 90 K in $\rho(T)$ of a *metallic* single crystal [9], suggesting that this sample exhibits a fully comparable magnetic transition and thus can be considered to represent stoichiometric $CaCrO_3$. But $\rho(T)$ of polycrystalline $CaCrO_3$ appears to be dominated by grain boundaries similar to the case of ferromagnetic metallic CrO_2, which also exhibits $\partial\rho/\partial T < 0$ in polycrystalline samples [21]. Presumably, the high valence of Cr^{4+} is not stable at the surface of a grain.

In contrast to dc transport, optical data can reveal the metallic properties of a polycrystalline sample with insulating grain boundaries. The reflectivity $R(\omega)$ extrapolates to 1 for $\omega \to 0$ (see Fig. 3), implying 3D metallic behavior.

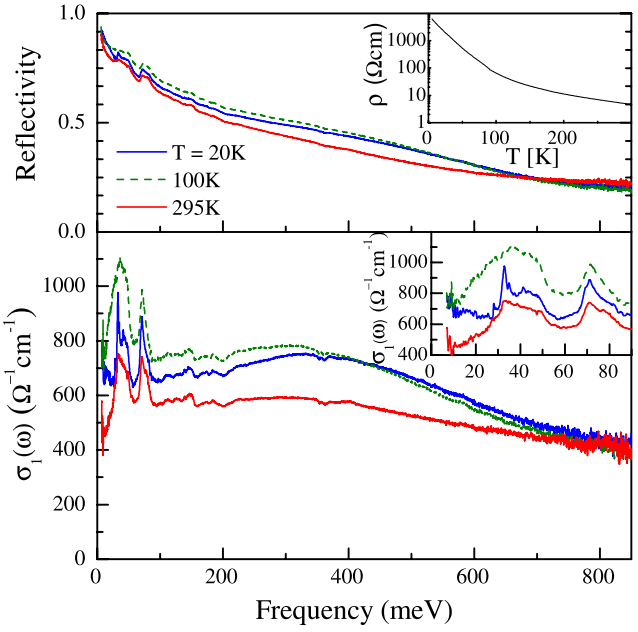

FIG. 3 (color online). Reflectivity (top) and optical conductivity $\sigma_1(\omega)$ (bottom). The inset in the bottom panel shows $\sigma_1(\omega)$ at low frequencies on an enlarged scale; the inset in the top panel depicts the resistivity $\rho(T)$.

In contrast, $R(\omega)$ extrapolates to a value much smaller than 1 in an insulator or a polycrystalline sample of a low-dimensional metal. In the case of insulating grain boundaries, $R(\omega)$ is suppressed at very low frequencies, where the wavelength is much larger than the typical grain size ($\sim$20 μm). However, for a stack of metallic grains and insulating boundaries [22] with a length ratio of 1000:1 or larger, the suppression of $R(\omega)$ is significant only below the lower limit of our experiment, 7 meV. Phonons are observed between 20 and 80 meV, and in $R(\omega)$ they are strongly screened by the itinerant charge carriers. Metallic conductivity further agrees with the magnetic susceptibility, which above T_N is very small and hardly temperature dependent, indicating itinerant magnetism [see Fig. 2(b)].

For the analysis of $R(\omega)$, we first assume that the optical conductivity $\sigma_1(\omega)$ is isotropic. In this case, $\sigma_1(\omega)$ can be derived via a Kramers-Kronig analysis of $R(\omega)$. We find a moderate conductivity with $\sigma_1(\omega)$ of the order of a few hundred to 1000 $(\Omega\ \mathrm{cm})^{-1}$ (see Fig. 3). The frequency dependence deviates strongly from a typical Drude behavior, as the spectral weight is dominated by a peak at about 350 meV. An increase of $\sigma_1(\omega)$ with decreasing frequency is recovered only below 30 meV at 20 K. If $\sigma_1(\omega)$ is strongly anisotropic, $R(\omega)$ represents an average over the different orientations of the grains, and the Kramers-Kronig analysis may produce a peak at finite frequencies although the individual components show conventional Drude behavior [23]. We emphasize that we obtain a reasonable description of $R(\omega)$ only for $\sigma_1(\omega) \gtrsim 200\ (\Omega\ \mathrm{cm})^{-1}$ for each direction. Furthermore, the Wannier function projection procedure within an LDA calculation predicts that the nearest-neighbor hopping matrix elements differ only by $\sim$10% between the c axis and the ab plane; thus, a pronounced anisotropy of $\sigma_1(\omega)$ is very unlikely. We tentatively attribute the peak at 0.35 eV to excitations from the lower (LHB) to the upper (UHB) Hubbard band. Because of the high valence of Cr^{4+}, the Cr Hubbard bands shift down towards the fully occupied $O-2p$ band, whereas the pd hybridization between Cr and O bands pushes the LHB back upwards, reducing the effective Coulomb repulsion U_{eff} [24] and admixing $O-2p$ states to the LHB and the UHB in the same way as it was demonstrated for CrO_2 [15].

In insulating Sr_2CrO_4 with d^2 Cr^{4+} [16], this LHB-UHB excitation was observed at 1.0 eV. Integrating $\sigma_1(\omega)$ from 7 meV to 0.9 eV in $CaCrO_3$ yields an effective carrier density $N \approx 0.1$ per Cr ion. Remarkably, this is very similar to the spectral weight of the LHB-UHB peak in Sr_2CrO_4 [16]. From a conventional Drude-Lorentz fit we estimate that the spectral weight of the free-carrier Drude contribution is about 5% of the total weight at 20 K. Apparently, $CaCrO_3$ is very close to a localized-itinerant crossover. Compared to layered Sr_2CrO_4, we attribute its metallic behavior to the 3D crystal structure inducing larger band widths and thus smaller U_{eff}.

To further analyze the electronic structure, we carried out *ab initio* band structure calculations for the $T = 3.5$ K

crystal structure within the LSDA approximation using the linear muffin-tin orbitals method [25]. Exchange constants were computed from the total energies of different magnetic solutions. In LSDA, $CaCrO_3$ is metallic in all studied magnetic structures: FM, AFM-G (all NN spins antiparallel), AFM-A (AFM coupled FM ab planes) and two AFM-C types with FM chains running in different directions. In agreement with experiment, the AFM-C structure with FM chains running along c has the lowest energy. The calculated magnetic moment is $\mu = 1.52\mu_B$/Cr, in good agreement with the measured value of $1.2\mu_B$. The reduction from $2\mu_B$ expected for localized Cr^{4+} ($S = 1$) is due to the strong pd hybridization. The further reduced experimental value can be ascribed to quantum fluctuations and the use of the form factor for localized Cr moments.

The exchange parameters explain the apparently anisotropic magnetic structure. We find a strong AFM exchange $J = 80$ K between NN spins within the ab plane [see Fig. 2(a)]. Surprisingly, also the NN exchange along c is AFM and only slightly smaller, $J' = 60$ K, although the experiment finds FM ordering in this direction. Its cause resides in a remarkably strong AFM NNN exchange $J'' = 33$ K along the diagonal. Since $J' < 4J''$, the AFM J' is overruled. Thus the C-type structure develops due to strong NNN interactions despite nearly isotropic NN interactions. The subtle balance of competing interactions may give rise to strong magnetoelastic coupling, explaining the pronounced structural anomalies at T_N. The flattening of the octahedron enhances the d_{xy} occupation thereby increasing J and—more importantly—decreasing J'. Note that magnetic interactions in the LSDA approach are due to the band magnetism of itinerant electrons. Therefore, the rather large NNN exchange is due to strong pd hybridization.

To check the importance of electronic correlations, we also performed LSDA + U calculations [26] where the on-site Coulomb interaction $U = 3$ eV and the Hund's rule coupling $J_H = 0.87$ eV were set to the values calculated for CrO_2 [15]. Also in LSDA + U the ground state is C-type AFM, but the electronic state is very different. In LSDA + U, $CaCrO_3$ is an insulator with a gap of $E_g \sim 0.5$ eV (due to the static approximation of the Coulomb correlations LSDA + U tends to overestimate E_g, and more sophisticated methods, like DMFT, may be needed). In the LSDA + U approach, the C-type magnetic structure is associated with orbital ordering: one electron localizes in the xy orbital at each Cr site and provides the in-plane AFM interaction, the second electron occupies alternating $1/\sqrt{2}(xz + yz)$ and $1/\sqrt{2}(xz - yz)$ orbitals. According to the Goodenough-Kanamori-Anderson rules this causes a FM interaction along c. This state is very similar to the one reported for insulating YVO_3 with G-type orbital order causing C-type magnetism [11,27]. We have searched for the orbital-order superstructure reflections in $CaCrO_3$ by high-flux powder neutron diffraction but did not find them although superstructure reflections 10^3 times weaker than a strong fundamental reflection would have been observed. Furthermore, a free refinement of the orbital-order model with the high resolution SPODI data does not yield any evidence for orbital ordering. We may thus exclude an orbital order comparable to that in YVO_3 for $CaCrO_3$. Still electronic correlations are important in $CaCrO_3$ driving it close to a metal-insulator crossover.

Summarizing our diffraction, macroscopic, and optical studies, we conclude that $CaCrO_3$ is a metallic and antiferromagnetic transition-metal oxide. There are other metallic antiferromagnetic oxides known, but these exhibit a reduced electronic and structural dimensionality rendering $CaCrO_3$ unique. The anisotropic C-type magnetic structure is explained by frustrating NNN (diagonal) interactions. Apparently, the magnetic interactions in $CaCrO_3$ are governed by sizable pd hybridization, a generic consequence of the high oxidation state associated with a small or negative charge-transfer gap.

This work was supported by the Deutsche Forschungsgemeinschaft through SFB 608 and by the Dynasty Foundation and via projects RFFI-07-02-00041, INTAS 05-109-4727, CRDF Y4-P-05-15, and MK-1184.2007.2.

[1] J. B. Goodenough, *Magnetism and the Chemical Bond* (Interscience publishers, New York-London, 1963).
[2] D. I. Khomskii and G. A. Sawatzky, Solid State Commun. **102**, 87 (1997).
[3] D. N. Argyriou *et al.*, Phys. Rev. B **59**, 8695 (1999).
[4] Y. Yoshida *et al.*, Phys. Rev. B **72**, 054412 (2005).
[5] J.-S. Zhou *et al.*, Phys. Rev. Lett. **96**, 046408 (2006).
[6] A. J. Williams *et al.*, Phys. Rev. B **73**, 104409 (2006).
[7] B. L. Chamberland, Solid State Commun. **5**, 663 (1967).
[8] J. B. Goodenough *et al.*, Mater. Res. Bull. **3**, 471 (1968).
[9] J. F. Weiher *et al.*, J. Solid State Chem. **3**, 529 (1971).
[10] L. Ortega-San-Martin *et al.*, Phys. Rev. Lett. **99**, 255701 (2007).
[11] Y. Ren *et al.*, Nature (London) **396**, 441 (1998).
[12] G. Cao *et al.*, Phys. Rev. B **56**, 321 (1997).
[13] J. Zaanen *et al.*, Phys. Rev. Lett. **55**, 418 (1985).
[14] D. I. Khomskii, Lithuanian J. Physics **37**, 65 (1997); see also arXiv:cond-mat/0101164.
[15] M. A. Korotin *et al.*, Phys. Rev. Lett. **80**, 4305 (1998).
[16] J. Matsuno *et al.*, Phys. Rev. Lett. **95**, 176404 (2005).
[17] A. C. Komarek *et al.*, Phys. Rev. B **75**, 224402 (2007).
[18] M. Braden *et al.*, Phys. Rev. B **58**, 847 (1998); O. Friedt *et al.*, Phys. Rev. B **63**, 174432 (2001).
[19] A. Liebsch and H. Ishida, Phys. Rev. Lett. **98**, 216403 (2007).
[20] E. F. Bertaut, Acta Crystallogr. Sect. A **24**, 217 (1968).
[21] J. Dai *et al.*, Appl. Phys. Lett. **77**, 2840 (2000).
[22] M. Grüninger *et al.*, Phys. Rev. Lett. **84**, 1575 (2000).
[23] J. Orenstein and D. H. Rapkine, Phys. Rev. Lett. **60**, 968 (1988).
[24] A. Gössling *et al.*, Phys. Rev. B **77**, 035109 (2008).
[25] O. K. Andersen and O. Jepsen, Phys. Rev. Lett. **53**, 2571 (1984).
[26] V. I. Anisimov *et al.*, Phys. Rev. B **44**, 943 (1991).
[27] G. R. Blake *et al.*, Phys. Rev. Lett. **87**, 245501 (2001).